NASA TECHNICAL NOTE

NASA TN D-5690

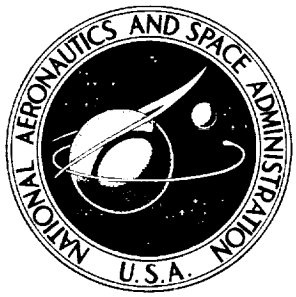

NASA TN D-5690

EXPERIMENTAL FLOW CHARACTERISTICS OF A SINGLE TURBULENT JET IMPINGING ON A FLAT PLATE

by Peter Hrycak, David T. Lee, James W. Gauntner, and John N. B. Livingood

Lewis Research Center
Cleveland, Ohio

NATIONAL AERONAUTICS AND SPACE ADMINISTRATION • WASHINGTON, D. C. • MARCH 1970

1. Report No. NASA TN D-5690	2. Government Accession No.	3. Recipient's Catalog No.
4. Title and Subtitle EXPERIMENTAL FLOW CHARACTERISTICS OF A SINGLE TURBULENT JET IMPINGING ON A FLAT PLATE		5. Report Date March 1970 6. Performing Organization Code
7. Author(s) Peter Hrycak, David T. Lee, James W. Gauntner, and John N. B. Livingood		8. Performing Organization Report No. E-5239
9. Performing Organization Name and Address Lewis Research Center National Aeronautics and Space Administration Cleveland, Ohio 44135		10. Work Unit No. 720-03 11. Contract or Grant No.
12. Sponsoring Agency Name and Address National Aeronautics and Space Administration Washington, D.C. 20546		13. Type of Report and Period Covered Technical Note 14. Sponsoring Agency Code

15. Supplementary Notes

16. Abstract

An experimental study of the flow characteristics of a circular air jet impinging on a smooth flat plate is described. Jets issuing from circular nozzles 0.125, 0.250, and 0.375 inch (0.317, 0.635, and 0.952 cm) in diameter were considered. Nozzle Reynolds numbers ranged from 600 to 100 000, and the normal distance between the nozzle exit and the plate was varied from 2 to 30 nozzle diameters. Some of the flow characteristics studied were potential core length, velocity and pressure distributions through the jet, spread of the jet, and velocity decay along the jet axis.

17. Key Words (Suggested by Author(s))	18. Distribution Statement		
Impinging jets Flat plate Flow characteristics Experimental study	Unclassified - unlimited		
19. Security Classif. (of this report)	20. Security Classif. (of this page)	21. No. of Pages	22. Price*
Unclassified	Unclassified	33	$3.00

*For sale by the Clearinghouse for Federal Scientific and Technical Information Springfield, Virginia 22151

EXPERIMENTAL FLOW CHARACTERISTICS OF A SINGLE TURBULENT JET IMPINGING ON A FLAT PLATE

by Peter Hrycak*, David T. Lee†, James W. Gauntner, and John N. B. Livingood

Lewis Research Center

SUMMARY

An experimental study of the flow characteristics of a circular air jet impinging on a smooth flat plate is described. Jets issuing from circular nozzles 0.125, 0.250, and 0.375 inch (0.317, 0.635, and 0.952 cm) in diameter were considered. Nozzle Reynolds numbers from 600 to 100 000 were studied, and the normal distance between the nozzle exit and the plate was varied from 2 to 30 nozzle diameters.

The effect of nozzle exit Reynolds number Re_o on potential core length was studied extensively. Maximum values were found at Re_o = 1000; sharp decreases followed until Re_o reached values between 3500 and 5500. A slight increase in potential core length was then observed until Re_o reached 10 000. Beyond Re_o = 10 000, the potential core length remained nearly constant and agreed well with the median value of other investigators. Experimentally determined velocity profiles agreed well with theoretically calculated distributions and with experiments of others for both the free jet and wall jet regions. Static-pressure distributions along the jet centerline varied from ambient pressure by 4 percent, at the most, which was in reasonable agreement with the usual theoretical assumption of constant static pressure in this region. Results also indicated that the nozzle-to-plate spacing has more influence on the static-pressure distribution along the impingement plate in the deflection region than either nozzle diameter or nozzle exit Reynolds number.

A theoretical derivation based on a method previously used for a two-dimensional nozzle and an empirical equation for the maximum velocity decay for a radial wall jet are presented for the circular nozzle. Good agreement between theory and experiment was achieved. An empirical relation for the spread of the wall jet is also included.

---

* Professor of Mechanical Engineering, Newark College of Engineering.

† Graduate student, Newark College of Engineering, now at Georgia Institute of Technology.

INTRODUCTION

An experimental study of the flow characteristics of a single circular jet impinging on a flat plate is reported. The investigation was performed at the Newark College of Engineering under NASA Grant NGR31-009-004.

The use of air jets impinging on the internal surfaces of turbine vanes and blades is a promising method for cooling such surfaces. In the development of adequate design heat-transfer correlations for this type of cooling, a detailed knowledge of the jet flow characteristics is necessary. Results obtained for single jets impinging on flat surfaces may prove useful for more complicated flows and geometries such as multiple jets impinging on either flat or curved surfaces.

A survey of previous investigations of single circular jets and slot jets is presented in reference 1. Areas requiring further investigation are discussed in the reference. These include the effect of nozzle Reynolds number on potential core length, the minor discrepancies between theoretical and experimental pressure profiles and between the assumed theoretical and experimentally determined wall velocity gradients. Reference 1 also discusses the application of jet flow characteristics to heat-transfer studies.

Herein, an extensive investigation was made of the effects of nozzle Reynolds number on potential core length. An analytical derivation of the relation for the maximum velocity decay of a radial wall jet is also presented. In the present experiments, the nozzle Reynolds numbers ranged from as low as 600 to as high as 100 000, and the normal distance between the exit of the nozzle and the plate varied from 2 to 30 nozzle diameters in order to observe the influences of varying Reynolds number and normal distance on the flow parameters. The smallest distance was restricted to two diameters because at this or smaller spacings readings at the nozzle exit are affected by the flat plate. Three nozzle diameters, 0.125, 0.250, and 0.375 inch (0.317, 0.635, and 0.952 cm), were investigated. Velocities and pressures between the nozzle and plate and along the plate were measured. Data from the investigation reported herein were also used in reference 2.

For the highest Reynolds numbers, Mach numbers approaching 0.5 were reached. Because of these large Mach numbers, compressibility corrections in the evaluation of instrument readings were required.

APPARATUS AND PROCEDURE

A schematic diagram of the apparatus is shown in figure 1. Air supplied by a compressor flowed through a filter and oil separator into a large storage tank to provide a

steady flow. From this tank, the air flowed through a feed pipe into a large plenum chamber. An end plate was welded to the end of the plenum chamber and equipped so that three different sized nozzles could be screwed to the end of the plate with a rubber ring to prevent air leakage. The nozzle diameters were 0.125, 0.250, and 0.375 inch (0.317, 0.635, and 0.952 cm).

The test plate was a flat 10-inch- (25.4-cm-) diameter smooth plate. The plate was supported by a three-leg frame that allowed the plate to be rotated or raised or lowered. Nineteen 1/64-inch- (0.04-cm-) diameter holes were drilled in the plate to accommodate taps for measuring the pressure distribution along the plate. Normal alinement of the air jet to the test plate was achieved by adjusting three plenum chamber supporting guide wires.

The air flow rate was controlled by valves and measured with rotameters with a calibrated accuracy greater than 99 percent. The inlet pressure at the rotameter inlet

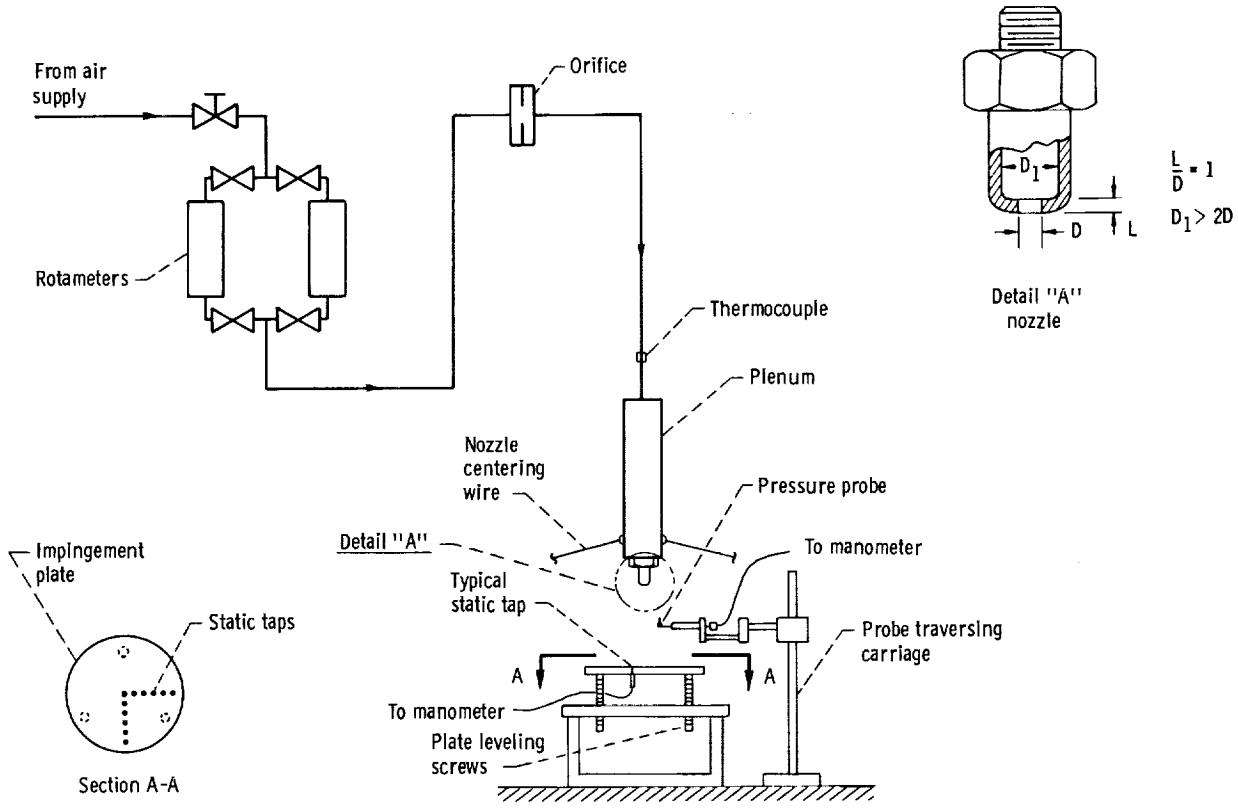

Figure 1. - Test apparatus.

was registered on a Bourdon-type pressure gage. Air temperature was measured by copper-constantan thermocouples upstream of the plenum chamber. Static- and total-pressure probes and microtubing pressure taps (0.016 in. or 0.04 cm) were used for pressure measurements. The static-pressure probe was constructed of 1/32-inch (0.08-cm) tubing and contained four 1/64-inch (0.04-cm) holes. The total-pressure probes were made from 1/64-inch (0.04-cm) tubing. For boundary layer thickness measurements, the total-pressure probe was flattened to 0.008 inch (0.02 cm) on the narrower side. The pressure probes were mounted on a traversing carriage so that they could be moved in three directions or rotated. U-tube water and mercury manometers were used for measuring pressures. For low-pressure measurement, a micromanometer, adjustable to within 0.001 inch (0.0025 cm), using a fluid with a specific gravity of 0.7970 was used.

The apparatus was equipped with a smoke generating device at the nozzle exit to achieve a visual picture of the flow to determine transition from laminar to turbulent flow.

Initial tests for velocity profiles at the nozzle exit revealed that the average exit nozzle velocity was 96 percent of the maximum nozzle exit centerline velocity. All tests were performed with the nozzle kept vertical to the impingement surface.

The impingement plate was maintained in a horizontal position. For assurance that the motion of the probes was along the line joining the center of the nozzle and the stagnation point, the jet centerline was alined with the stagnation point on the plate. This alinement was accomplished by following a suggestion discussed by Lee (ref. 2). A drop of dark grease applied at the approximate stagnation point spread out radially and made it possible to observe streamlines and the stagnation point. The probe was then lowered to the impingement plate to ensure that it coincided with the stagnation point.

Test conditions for the experiments described in this report are summarized in table I. Figure 2, reproduced from reference 1, shows the four regions into which the impinging jet is divided. For determination of jet centerline velocity and pressure distributions, a range of Reynolds numbers was investigated. For the nozzle with a diameter of 0.125 inch (0.317 cm), 23 different values of Re_o ranging from 620 to 45 000 were considered. For the 0.250-inch (0.635-cm) nozzle diameter, 27 Reynolds numbers ranging from 1250 to 100 000 were studied. For the largest nozzle, 24 values of Re_o ranging from 930 to 100 000 were tested. Centerline measurements of static and total pressures were made at various locations from the nozzle with values of the ratio of the distance from the nozzle to the nozzle diameter x/D up to 40, 28, and 24 for nozzle diameters of 0.125, 0.250, and 0.375 inch (0.317, 0.635, and 0.952 cm), respectively.

Transverse measurements in the jet were made using the 0.250-inch (0.635-cm) nozzle for values of the ratio of the distance from the jet centerline to the nozzle diameter y/D from 0 to a maximum of 5 for regions I and II (see fig. 2). Nozzle-to-plate

TABLE I. - TEST CONDITIONS

	Nozzle diameter, D		
	0.125 in. (0.317 cm)	0.25 in. (0.635 cm)	0.375 in. (0.952 cm)
Nozzle Reynolds number, Re_o	620 to 45 000 (23 values)	1250 to 100 000 (27 values)	930 to 100 000 (24 values)
Distance from nozzle to plate, z_n/D	2, 4, 7, 10, 14, 20	4, 7, 10, 20, 30	4, 7, 10, 20, 30
Centerline measurement stations, x/D	0 to 40	0 to 28	0 to 24
Transverse measurement stations, y/D	----------	0 to 5	----------
Plate measurement stations, r/D	0 to 24	0 to 28	0 to 12

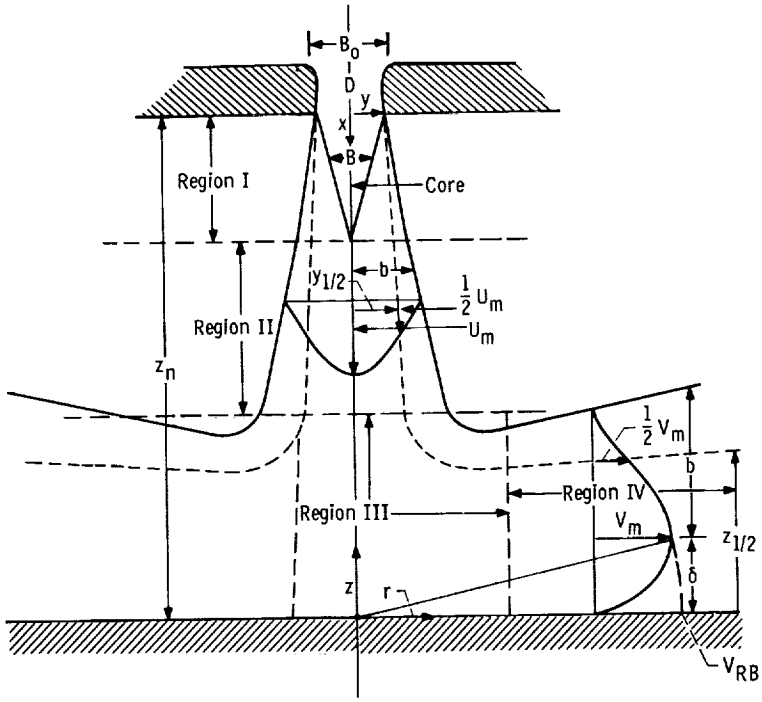

Figure 2. - Characteristic regions in impinging jet flow.

spacings z_n/D ranged from 2 to 30. Not all the aforementioned values of Reynolds number were considered for each value of y/D or z_n/D just cited.

Static-pressure measurements along the impingement plate were made at values of the ratio of the radial distance from the stagnation point to the nozzle diameter r/D ranging from 0 to 24, 28, and 12, respectively, for the nozzles in the order of increasing diameter size. Velocity profiles through the wall jet (region IV) were also determined for both the 0.25- and the 0.375-inch- (0.635- and 0.972-cm-) diameter nozzles and for values of z_n/D of 7 and 10 at distances from the jet centerline of 2, 2.5, 3, and 3.5 inches (5.08, 6.35, 7.62, and 8.89 cm) for several Reynolds numbers.

RESULTS AND DISCUSSION

Observations of Smoke Flow Tests

Flow patterns were observed by means of smoke at low Reynolds numbers. Beginning with $Re_o = 1000$, the flow was laminar to a distance of about four nozzle diameters from the nozzle exit. Downstream of this location, some small turbulence occurred on the boundary of the free jet with the quiescent surroundings. When the Reynolds number was increased, the extent of the laminar flow was reduced and more turbulence existed. Finally, at a Reynolds number near 4000, the jet was fully turbulent. This observation helps to explain why a relatively long length of the potential core exists at $Re_o = 1000$ and then decreases in length as Re_o approaches 4000. A detailed discussion of potential core length is given in the next section.

Region of Flow Establishment (Region I)

Length of potential core. - The fundamental interest in region I is to determine the length of the potential core. For this determination, the velocity decay along the centerline of the jet in the region of established flow (region II) was plotted against the dimensionless distance from the nozzle x/D on log-log paper. The intersection of the line representing this centerline velocity decay with the horizontal line representing the dimensionless centerline velocity in region I $U_m/U_{o,c} = 1$ defines the potential core length C_2.

Centerline velocity values were determined experimentally for nozzles with diameters of 0.125, 0.250, and 0.375 inch (0.317, 0.635, and 0.952 cm) for a range of Reynolds numbers. The results for the 0.125-inch- (0.317-cm-) diameter nozzle are plotted in figure 3. As just stated, the intersection of a velocity decay line with the line

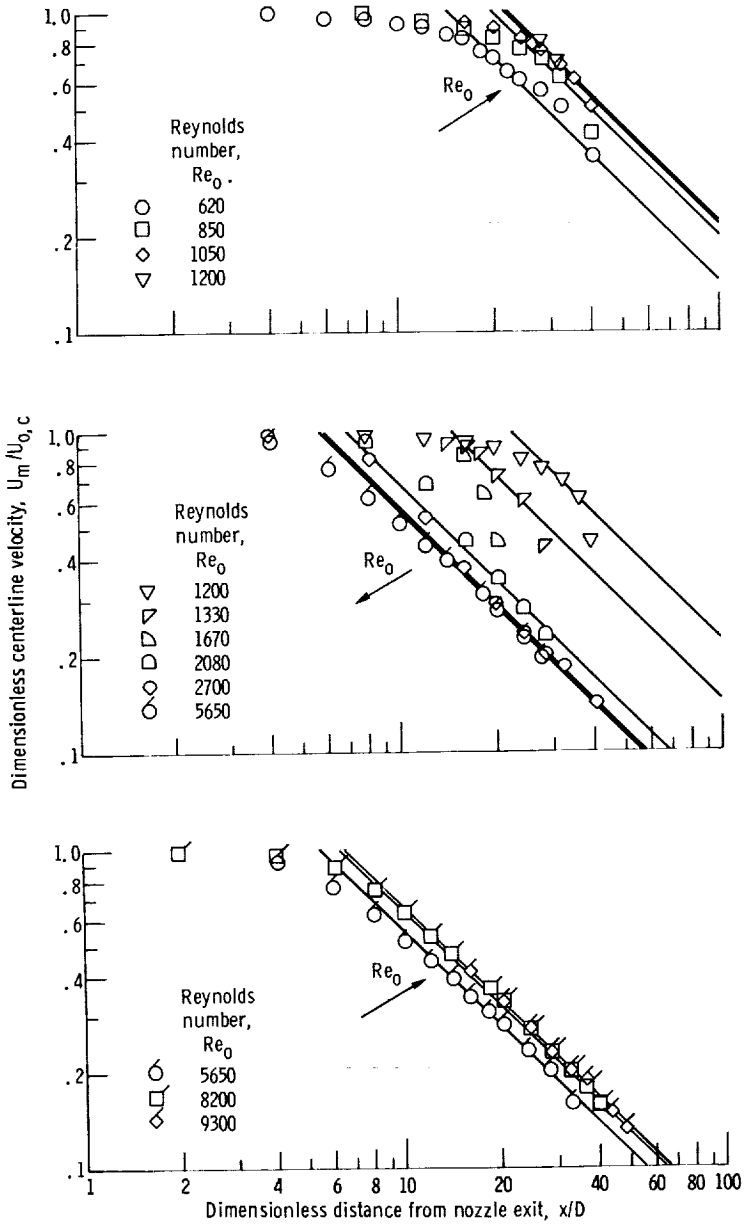

Figure 3. - Centerline velocity decay for 0.125-inch- (0.317-cm-) diameter nozzle.

$U_m/U_{o,c} = 1$ determines the length of the potential core. The figure shows the fluctuating value of the potential core length as the Reynolds number is varied over a wide range of values. Similar results were obtained for the other two nozzles.

Values of the potential core length plotted against Re_o for the three nozzles are shown in figure 4. The figure shows that initially, as the jet remains laminar, the potential core length is proportional to the Reynolds number, in accordance with equation (23) of reference 1. In general, C_2 reaches a maximum at a value of Re_o of about 1000. For values of Re_o between 1000 and 10 000 (transition flow), large fluctuations in potential core length are shown. For $Re_o > 10\ 000$, the potential core length remains essentially constant. Because the air velocities involved are for large Reynolds num-

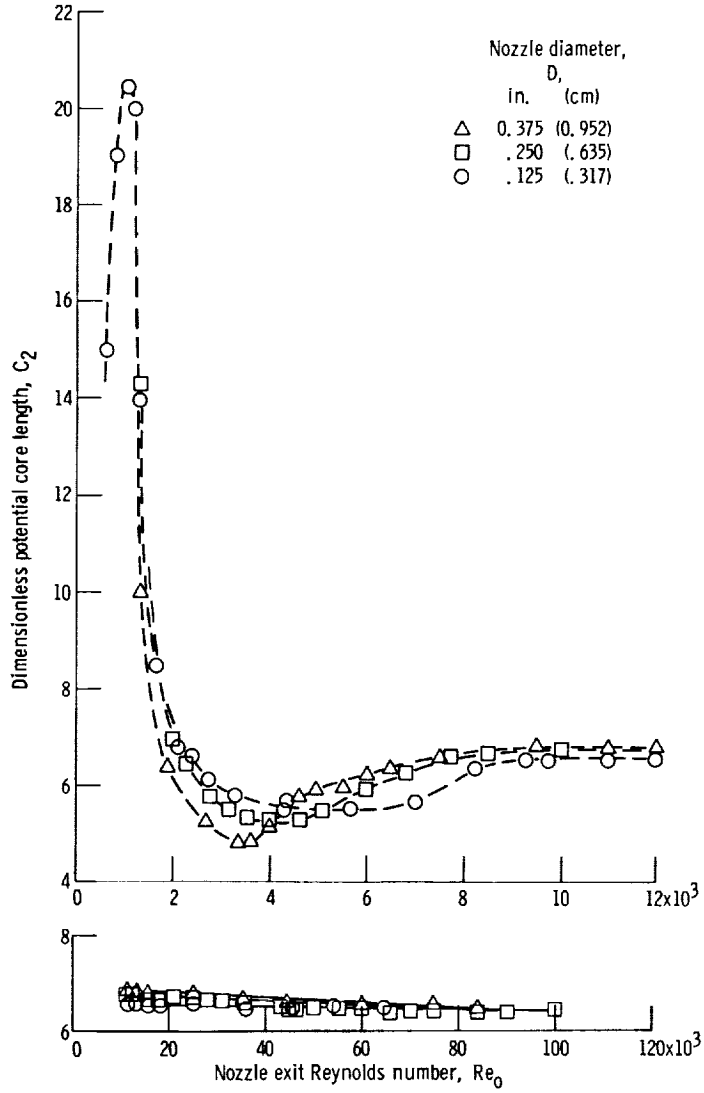

Figure 4. - Variation of potential core length with Reynolds number.

bers (to 100 000), the Mach numbers approach 0.5 and compressibility corrections are required; when these corrections are applied, the potential core length becomes independent of the Reynolds number for Reynolds numbers greater than 10 000, in accordance with equation (26) of reference 1 for fully developed turbulent flow. From figure 4, the minimum values of C_2 were 4.8 at $Re_o = 3500$ for $D = 0.375$ inch (0.952 cm), 5.3 at $Re_o = 4000$ for $D = 0.250$ inch (0.635 cm), and 5.5 at $Re_o = 5500$ for $D = 0.125$ inch (0.317 cm). The maximum values were 6.8, 6.75, and 6.5 at about $Re_o = 10\,000$, respectively, for the three nozzles. These results compare well with the median of the results of other investigators; namely, $C_2 = 6.1$, as noted in reference 1.

According to reference 3, C_2 is not a function of Reynolds number in the range from 20 000 to 4 000 000. The present results show, however, a weak dependence of C_2 on Reynolds number for Re_o greater than 10 000. Reference 2 shows that this dependence on Reynolds number for Re_o greater than 20 000 disappears if compressibility corrections are carried out. The present results likewise show a strong dependence of C_2 on Reynolds number for Re_o less than 10 000. This dependence is very strong near $Re_o = 1000$, which, by observation of flow patterns made visible by smoke, was the critical Reynolds number for the jet flow in the present investigation.

Figure 4 also shows a strong dependence of C_2 on the nozzle diameter for Re_o greater than 2000 but less than 10 000. Figure 4 also shows a weak dependence of C_2 on the nozzle diameter for Re_o greater than 10 000.

Velocity profile. - Velocity profiles at values of $x/D = 0$ and 4 are shown in figure 5. Data for the 0.25-inch- (0.634-cm-) diameter nozzle for a range of Reynolds numbers are presented. The figure shows the decrease in the potential core width and the increase in the jet width as the distance from the nozzle increases.

The velocity profile at $x/D = 4$, shown in figure 5, was selected for comparison with the prediction of Albertson et al. (ref. 4). This prediction method describes the profile to a first approximation as two symmetrical halves of the probability curve connected with a straight line through the constant velocity core; only the nonlinear part of the profile is considered. Comparing the data of figure 5 with the prediction necessitated that the boundary of the potential core be considered as the point $y = 0$. A value of $y_{1/2}$ (where $U/U_{o,c} = 1/2$) was determined, and abscissas corresponding to selected values of $U/U_{o,c}$ from the appropriate curve in figure 5 were determined. The results, plotted as the solid line in figure 6, are compared with the curve by Albertson et al. (ref. 4). The present results show some disagreement with that curve and follow the trend of the experimental points illustrated in figure 16 of reference 4. The reason for this apparent disagreement was the fact that Albertson et al. wanted to cover both the region of flow establishment and the region of developed flow using one and the same

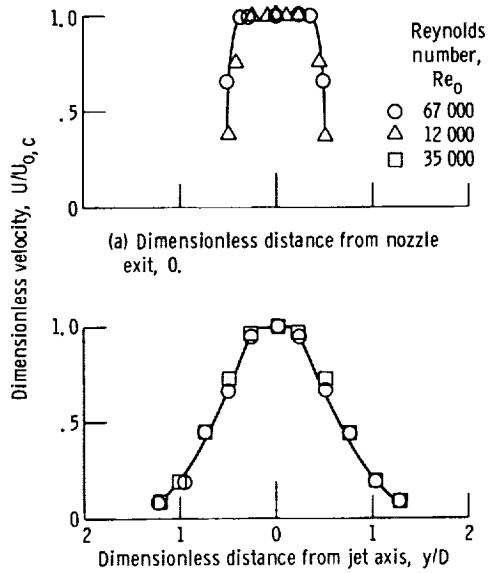

(a) Dimensionless distance from nozzle exit, 0.

(b) Dimensionless distance from nozzle exit, 4.

Figure 5. - Velocity profile in region I at dimensionless distances from nozzle exit of 0 and 4. Nozzle diameter, 0.25 inch (0.635 cm).

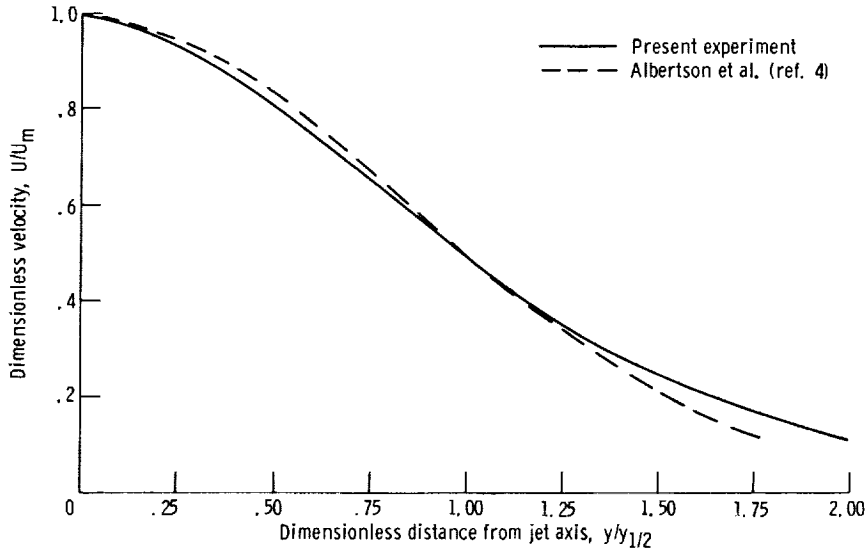

Figure 6. - Comparison of experimental velocity profile through region I with prediction.

experimental constant. Their own results prove that this cannot be done, and this conclusion is further supported by the results of the present investigation (compare eqs. (2) and (3) with (4) and (5) in the section Spread of jet).

Region of Established Flow (Region II)

Jet centerline velocity decay. - A curve showing the jet centerline velocity decay was discussed in connection with the determination of the potential core length. This curve is shown in figure 3 and confirms the statement made previously that the velocity decays in a manner inversely proportional to the distance from the nozzle in the region of developed flow for both the laminar and the turbulent flows.

Figure 7 shows the centerline velocity decay for various values of the distance between the nozzle and the plate for the largest diameter nozzle. Close examination of this figure verifies the fact that the jet behaves like a free jet except within a few nozzle diameters of the impingement plate. The nearly vertical linear portions are taken from reference 5, since in the present study the probes used prevented accurate measurements very near the plate.

If data like those presented in figure 4 are available, it is possible to evaluate the centerline jet velocity at any point in region II by use of equation (18) of reference 1:

$$\frac{U_m}{U_{o,c}} = \frac{C_2}{\frac{x}{D}} \tag{1}$$

In reference 1, $U_{o,c} = U_o$. All symbols are defined in appendix A.

Velocity profile. - The velocity profiles through region II for flow through the 0.25-inch- (0.635-cm-) diameter nozzle at distances of 8, 12, and 16 nozzle diameters from the nozzle are shown in figure 8 for two Reynolds numbers. A comparison of these curves with those of figure 5, which showed similar distributions at two positions within region I, indicates how the jet is spreading.

Data for the velocity profiles shown in figure 8 were replotted and compared with the theories of Tollmien (ref. 6) and Görtler (ref. 7). These theories were developed for free turbulent flows and, as such, are of a boundary layer nature; they are also discussed in reference 1. The first boundary layer solution (Tollmien, ref. 6) used Prandtl's mixing length theory; the other solution (Görtler, ref. 7) uses Prandtl's hypothesis that the virtual kinematic viscosity ϵ is a constant. Figure 9 shows this comparison of data with theory and indicates that the theories predict the velocity profile well. This fact was also confirmed by other investigators, as reported in reference 1.

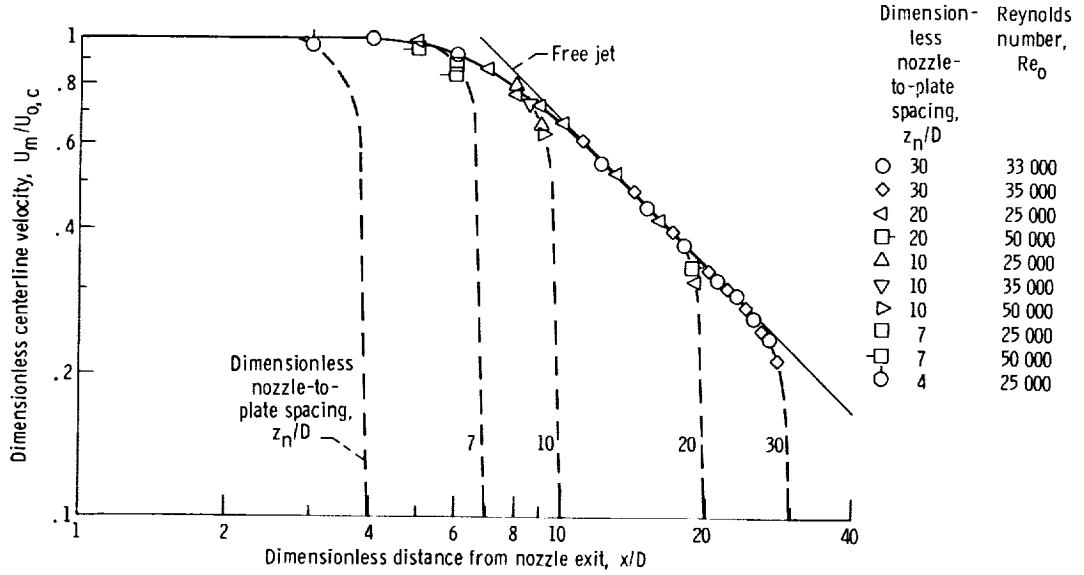

Figure 7. - Centerline velocity decay with various values of dimensionless nozzle-to-plate spacing and Reynolds number. Nozzle diameter, 0.375 inch (0.952 cm).

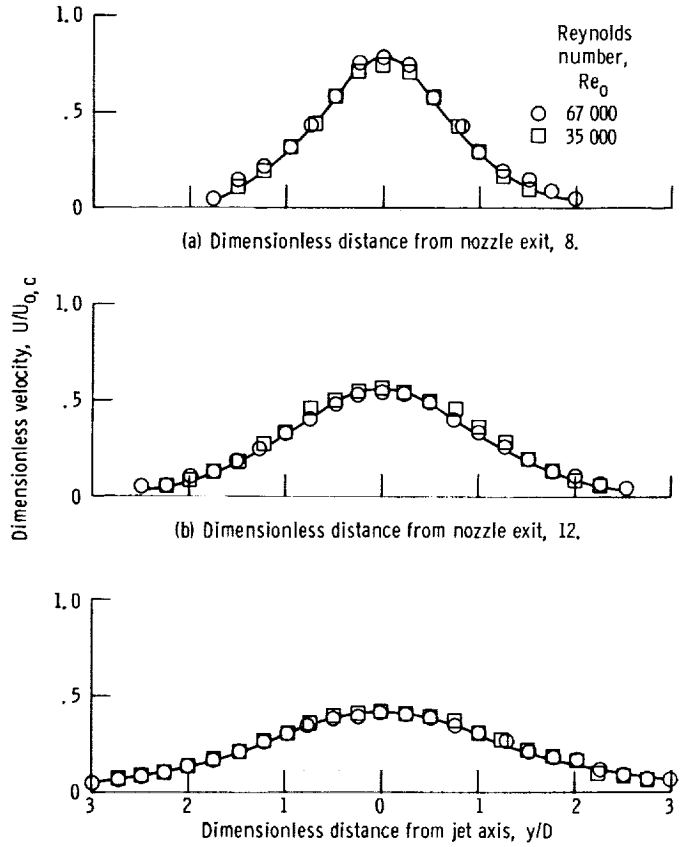

(a) Dimensionless distance from nozzle exit, 8.

(b) Dimensionless distance from nozzle exit, 12.

(c) Dimensionless distance from nozzle exit, 16.

Figure 8. - Velocity profile in region II at three dimensionless distances from nozzle exit. Nozzle diameter, 0.250 inch (0.635 cm).

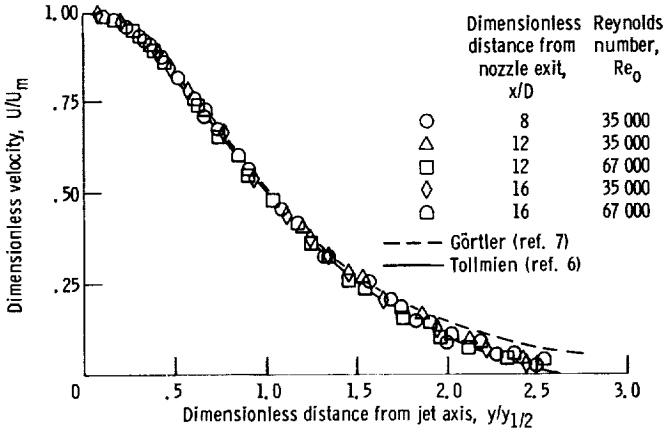

Figure 9. - Comparison of experimental velocity profile through region II with theory. Nozzle diameter, 0.250 inch (0.635 cm).

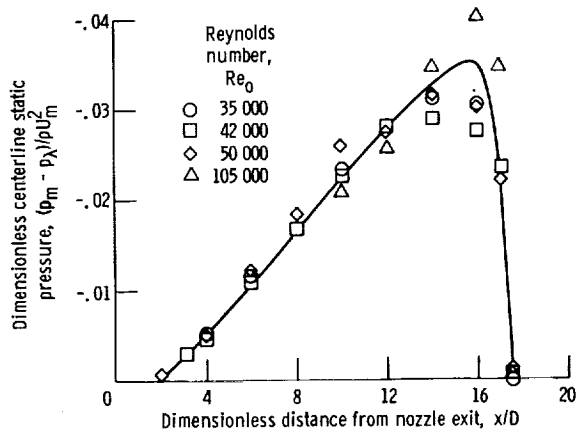

Figure 10. - Pressure distribution along centerline of free jet. Nozzle diameter, 0.25 inch (0.635 cm); dimensionless nozzle-to-plate spacing, 20.

Jet centerline pressure variation. - Experimental values of the jet centerline static pressure were measured as a function of distance from the jet nozzle. This centerline pressure decreased below ambient pressure a few nozzle diameters downstream of the jet exit. It continued to decrease with increasing distance from the nozzle until a minimum was reached downstream of the potential core region. At this point, the pressure started to increase and approached ambient pressure. These tests were performed for three different nozzle diameters with the point of minimum static pressure occuring slightly farther downstream with increasing nozzle size.

Figure 10 shows a plot of the static pressure along the jet centerline for the 0.25-inch- (0.635-cm-) diameter nozzle when the plate-to-nozzle spacing is 20 nozzle diameters. In theoretical studies based on similar solutions (velocity profiles at different positions differ by a scale factor), the jet axial static pressure is assumed constant. Figure 10 shows a maximum variation of about 4 percent for the centerline static-pressure variation, a result in reasonable agreement with the usual theoretical assumption.

Static-pressure profiles. - An experimental static-pressure distribution of the jet in the transverse direction for a fixed nozzle-to-plate spacing and a fixed Reynolds number was also measured. The minimum pressure was observed at the jet centerline and gradually approached ambient pressure as the distance from the centerline increased. The results appear in figure 4.13 of reference 2 and approximately agree with those of Miller and Comings (ref. 8).

Spread of jet. - Data defining the spread of a free jet where y equals the half-width b and where y equals the half-velocity value $y_{1/2}$ are shown in figure 11 as solid lines. The dashed lines are the extensions of the solid lines for fully developed flow and

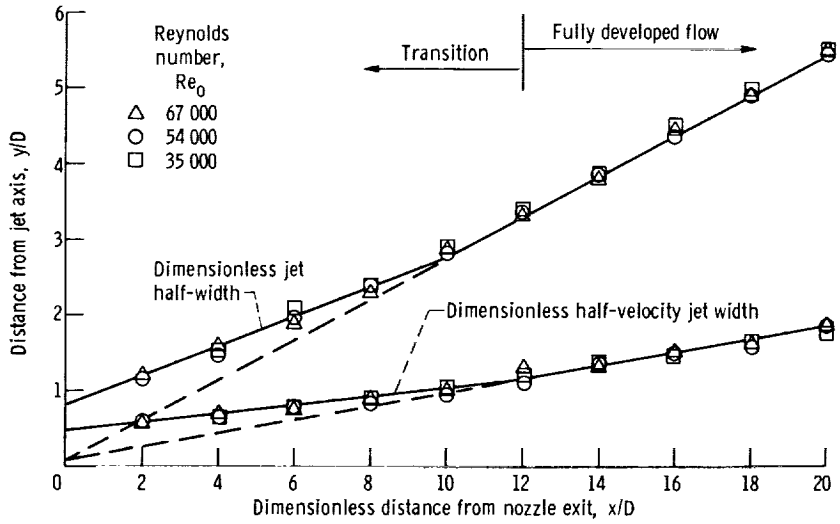

Figure 11. - Spread of jet. Nozzle diameter, 0.250 inch (0.635 cm).

emphasize that the rate of spread of the jet is smaller for transition than for fully developed flow. These extensions indicate the approximate location of the virtual origin. In the fully developed flow region, the data in figure 11 may be represented by

$$\frac{b}{D} = 0.271 \frac{x}{D} \tag{2}$$

and

$$\frac{y_{1/2}}{D} = 0.0926 \frac{x}{D} \tag{3}$$

for the jet half-width and jet width where $U = 0.5\ U_m$, respectively.

These equations indicate that the spreading of the jet is proportional to the distance from the nozzle. The coefficient in equation (3) is close to the value of 0.097 quoted by Abramovich (ref. 3). These equations only hold in the fully developed turbulent region for distances from the plate in excess of two nozzle diameters; within two nozzle diameters of the plate, the flow is influenced by the impingement plate (see fig. 7).

The corresponding equations for the jet half-width and width, where $U = 0.5\ U_m$ in the transition zone, can also be obtained from figure 11. For the jet half-width,

$$\frac{b}{D} = 0.1986 \frac{x}{D} + 0.763 \tag{4}$$

and for the width where $U = 0.5\ U_m$,

$$\frac{y_{1/2}}{D} = 0.0588 \frac{x}{D} + 0.466 \tag{5}$$

Deflection Region (Region III)

Velocity variation along jet centerline. - No measurements were made during the present investigation sufficiently close to the impingement plate to be considered in flow region III. However, the analysis in reference 9 indicated that the velocity distribution along the centerline in region III is given by the following relation for a distance of a few nozzle diameters from the plate:

$$U_m = -2a(z_n - x) \tag{6}$$

Obviously, at the plate where $x = z_n$, $U_m = 0$. For values of x close to z_n, the velocity is represented by a straight line with a slope that is $-2a$, where a is an empirical constant.

Maximum velocity variation along impingement plate. - As discussed in reference 1, a region exists adjacent to the stagnation point in which the viscous effects are negligible. As the viscous effects become more pronounced, the velocity profiles approach that of a fully developed wall jet. The maximum velocity in these profiles V_m can be expressed by

$$V_m = ar \tag{7}$$

If both sides of this equation are divided by $U_{o,c}$, the equation can be rewritten as

$$\frac{V_m}{U_{o,c}} = \frac{aD}{U_{o,c}} \frac{r}{D} = a^* \frac{r}{D} \tag{8}$$

This equation is the basis for the curves shown in figure 12. The measured maximum velocity variation along the impingement plate in the deflection region is shown in the figure; here, the ratio $V_m/U_{o,c}$ is plotted against r/D for four values of z_n/D and a nozzle diameter of 0.25 inch (0.625 cm). Also shown in the figure are curves calcu-

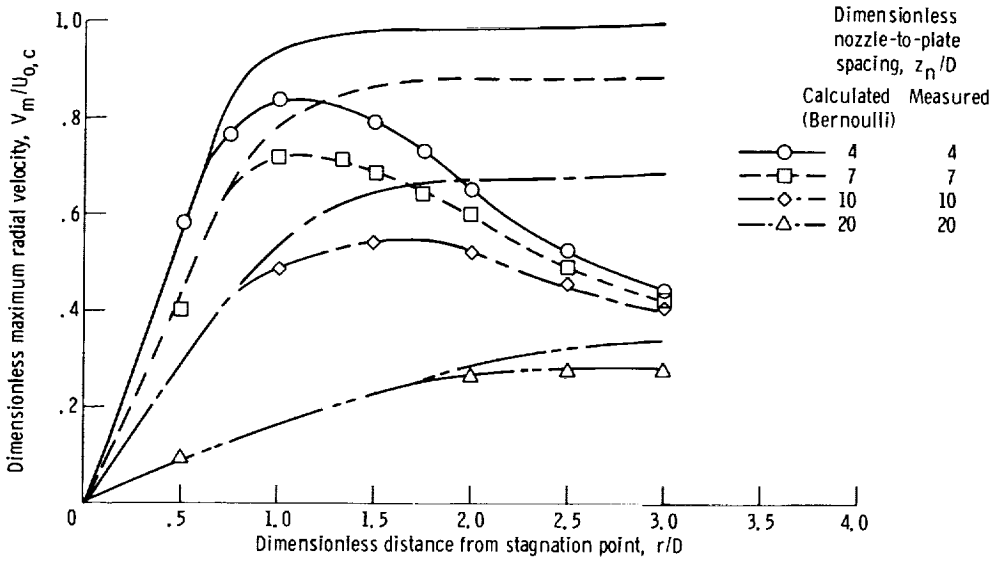

Figure 12. - Velocity variation in deflection region (region III). Nozzle diameter, 0.250 inch (0.635 cm).

lated from the measured static-pressure distribution by assuming no energy dissipation in the flow (i.e., by use of Bernoulli's equation):

$$p + \frac{1}{2}\rho V_m^2 = \text{constant}$$

The experimental data were obtained from the use of measured total stagnation point pressure and the static and total pressures measured along the line of maximum velocity. The data increase in velocity as r/D increases, reach a maximum, and then decay by energy dissipation. These results are similar to those presented in reference 5. Examination of figure 12 shows that the data and calculated curves agree from $r/D = 0$ to $r/D = 0.6$ or from $r/D = 0$ to $r/D = 1.4$, depending on the magnitude of z_n/D. For small values of r/D where viscous effects are negligible, the figure also shows that the slopes of the curves are a function of z_n/D. As the value of r/D increases, viscous effects increase, and the experimental data depart from the Bernoulli curves. The point where viscosity begins to have an effect is farther from the stagnation point as the nozzle-to-plate spacing increases.

Boundary layer development. - Total pressure was measured by use of an 0.008-inch (0.02-cm) probe throughout the boundary layer, while the static pressure was measured with the static-pressure probe with only the bottom hole left open, at various distances r from the stagnation point. The radial velocities were calculated from these pressure measurements, and velocity distributions were obtained. The value of the boundary layer thickness δ was then determined as the distance from the wall where $V/V_m = 1$. Plots of δ/D against r/D could then be made. Such plots are shown in

figure 13 for a Reynolds number of 54 000 and values of z_n/D of 3, 7, 10, and 20 for the 0.375-inch- (0.952-cm-) diameter nozzle. These experimental values of boundary layer thicknesses are considered to be accurate to within 0.002 inch (0.005 cm), which corresponds to an uncertainty of about 15 percent in δ/D for z/D of 20 in figure 13.

Schlichting (ref. 9) presents results of a theoretical investigation by Frössling of axially symmetric stagnation flow. Near the edge of the inner boundary layer, where $V = 0.99\ V_m$, the following equations are obtained with the aid of table 5-1 of Schlichting:

$$\frac{\delta}{D} = \frac{2.788}{\sqrt{a^* \, Re_o}} \tag{9}$$

where

$$a^* = \frac{aD}{U_{o,c}} \tag{10}$$

The term a^* can be evaluated from data like those presented in figure 12 and is equal to 0.1808 for $z_n/D = 20$. With this value of a^* and the value of $Re_o = 54\ 000$, a value of δ/D was calculated from the foregoing theoretical equation and was 0.02765. This value of δ/D may be compared with the directly measured value of 0.037 shown in figure 13. Since this velocity boundary layer thickness shown in the figure is for $V = V_m$, it should not be expected to compare favorably to Schlichting's value based on $V = 0.99\ V_m$. In fact, the measured value is 33 percent larger than the analytical value.

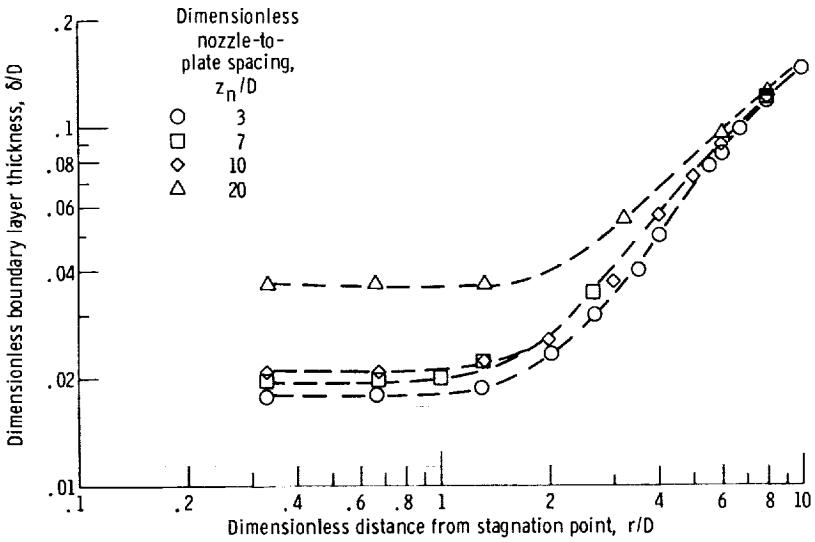

Figure 13. - Boundary layer development. Reynolds number, 54 000; nozzle diameter, 0.375 inch (0.952 cm).

Near the center of the deflection region, the experimental results agree qualitatively with theory, which strongly suggests the existence of laminar flow near the stagnation point for otherwise turbulent impinging jets; also, the experimental boundary layer thickness increases with increased spacing between the nozzle and the plate.

In the outer portion of the deflection region, the experimental boundary layer thickness becomes less dependent on nozzle-to-plate spacing and increases in thickness with distance from the stagnation point. This result is consistent with the theoretical predictions for the wall jet region.

Pressure distribution along impingement plate. - A pressure distribution along the impingement plate is shown in figure 14 for the 0.25- and 0.375-inch- (0.635- and 0.952-cm-) diameter nozzles, a range of Reynolds numbers, and values of z_n/D = 4, 7, 10, and 20. Since the nozzle diameter and the Reynolds number effects on the static pressure parameter are relatively insignificant (as can be seen in fig. 14 for the case with z_n/D = 4), a mean curve was drawn through the data. The curve shows a maximum value at the stagnation point (r/D = 0) and a rapid decrease followed by an asymptotic approach to zero; at a distance of r/D = 3, the curve is very near to the horizontal axis, and the pressure is about equal to the ambient pressure. Mean curves are also shown for measurements obtained with the other values of z_n/D. Both the slope and the maximum value increase as the value of z_n/D decreases.

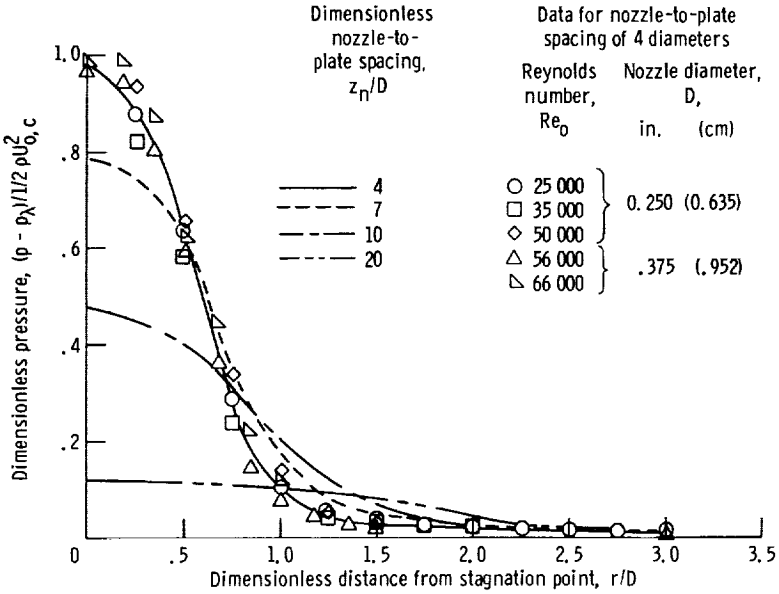

Figure 14. - Pressure distribution along impingement plate in region III.

Wall Jet Region (Region IV)

Maximum velocity decay along impingement plate. - The maximum velocity V_m is that velocity at the boundary between the two flow layers (one where the flow is influenced by the wall and the other where the flow behaves as a free jet). This use of two layers is discussed in reference 1.

What is apparently a new derivation for the maximum velocity decay for a radial wall jet is presented in appendix B. The analysis follows the method used by Abramovich in his study of the two-dimensional jet. It is based on the assumptions that the flow is incompressible (ρ = constant), the ambient fluid is stationary, the flow is in steady state, and the velocity distribution in the turbulent boundary layer is given by the well-known power law

$$\overline{V} = \overline{V}_m(\overline{z})^{1/n} \tag{11}$$

As shown in appendix B,

$$\overline{V}_m = \frac{\text{constant}}{\overline{r}^{(\alpha+1)\beta/2}\left(1 - \frac{\overline{r}_o}{\overline{r}}\right)^{\alpha\beta/2}} \tag{12}$$

where β is a function of n, which in turn is a function of Reynolds number. Far from the stagnation point, where $\overline{r} >> \overline{r}_o$, the maximum radial velocity decay reduces to

$$\overline{V}_m = \frac{\text{constant}}{\overline{r}^{\alpha_1}} \tag{13}$$

where

$$\alpha_1 = \frac{(\alpha + 1)\beta}{2}$$

and shows a slight dependence on Reynolds number.

When the ratio of the velocity V_m to that at the nozzle exit $U_{o,c}$ was plotted against r/z_n, for $\alpha_1 = 1.12$, a family of lines independent of Re_o was obtained for different values of z_n/D for the 0.25-inch- (0.625-cm-) diameter nozzle. The linear portions of these lines may be represented by the relation

$$\frac{V_m}{U_{o,c}} = \frac{1.4}{\left(\frac{z_n}{D}\right)^{1.12}\left(\frac{r}{z_n}\right)^{1.12}} \tag{14}$$

The data were replotted, as shown in figure 15, where the abscissa is r/D. The linear portion of the curve represents the maximum velocity decay as

$$\frac{V_m}{U_{o,c}} = \frac{1.4}{\left(\frac{r}{D}\right)^{1.12}} \tag{15}$$

The length of the deflection region for each value of z_n/D can be noted at that point where the curves fair into the linear portion.

It is interesting to note that when $\beta/2$ is calculated as a function of k (where $k = \delta/b$) and n for the experimentally verifiable values of $k = 1/9$ and $7.5 < n < 15$ (see fig. 4.35 of ref. 2), with $\alpha = 0.95$, the calculated value of α_1 compares very favorably with the experimentally obtainable result $\alpha_1 = 1.12$ for smooth plates. The value of the exponent 1.12 agrees quite well with values of previous investigators: Poreh et al. (ref. 10), 1.1; Brady and Ludwig (ref. 11), 1.14; and Bakke (ref. 12), 1.12.

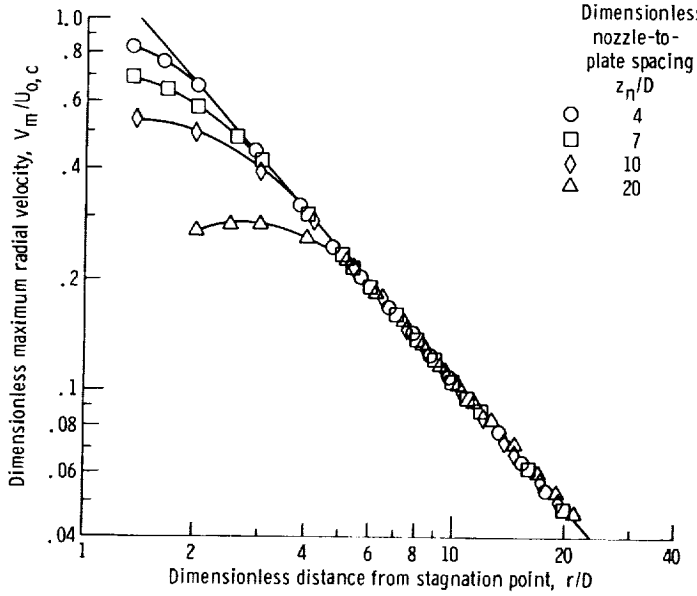

Figure 15. - Comparison of velocity variation in region IV for several values of dimensionless nozzle-to-plate spacing. Nozzle diameter, 0.250 inch (0.635 cm).

It should be noted that the power of r is greater than 1, and hence, the maximum velocity along the plate decays more rapidly than that of a free jet, which decays with the power 1 of r. It may also be shown that, in the absence of wall friction, the analytical expression for α_1, given in appendix B, reduces to 1.

Velocity profiles through wall jet region. - Dimensionless velocity profiles V/V_m are plotted in figure 16 against $z/z_{1/2}$, where $z_{1/2}$ is the value of z for which $V = \frac{1}{2} V_m$. The profiles are for $z_n/D = 10$ at 2 inches (5.08 cm) from the stagnation point and for a range of Reynolds number. Data for other values of z_n/D and other distances from the stagnation point show similar results. Careful inspection of the experimental data illustrates the validity of the wall jet velocity similarity law. Reynolds number effects, for all practical purposes, are limited to the immediate vicinity of the wall, where the profiles become flatter as the Reynolds number increases.

Comparison of these profiles with those of Glauert (ref. 13) show generally good agreement. This fact was also confirmed by other investigators, as reported in reference 1. The data shown herein reveal that the experimental profile is lower than

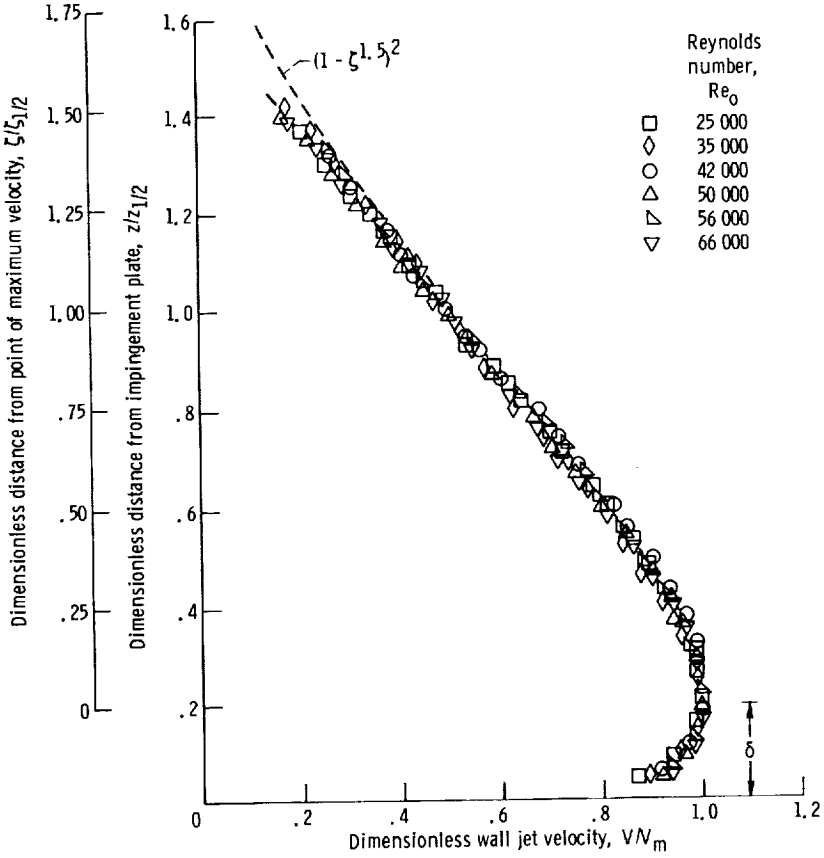

Figure 16. - Comparison of velocity profile of wall jet with theory of Abramovich. Distance from stagnation point, 2 inches (5.08 cm); nozzle diameter, 0.250 inch (0.635 cm); dimensionless nozzle-to-plate spacing, 10.

Glauert's in the outer portion of the jet and is flatter than Glauert's at the tip, but very similar to Bakke's (ref. 12) experimental profile.

Figure 16 also shows good agreement between the data and Abramovich's relation

$$\frac{V}{V_m} = \left(1 - \zeta^{3/2}\right)^2 \tag{16}$$

for values of $\zeta/\zeta_{1/2}$ to about 1.5. Equation (16) is valid only outside the inner turbulent boundary layer (note the scale for $\zeta/\zeta_{1/2}$ in fig. 16).

A plot of the reference velocity V_{RB}, as shown in figure 2 is presented in figure 17. The reference velocity is the centerline velocity at r of a hypothetical free jet issuing radially from the stagnation point, and it can be obtained by extrapolating the velocity profile of the outer jet zone to the wall. This extrapolation verifies that V_{RB} varies as $1/r$ in the wall jet region (region IV); present data fall on a curve, as shown in the figure, represented by

$$\frac{V_{RB}}{U_{o,c}} = \frac{0.62}{r/z_n} \tag{17}$$

Spread of wall jet. - The growth of the half-velocity width of the wall jet is shown in figure 18 for four values of $z_{1/2}/D$. Four distinct parallel lines are shown, one for each value of z_n/D. The lines may be represented by

$$\frac{z_{1/2}}{D} = K\left(\frac{r}{D}\right)^{0.95} \tag{18}$$

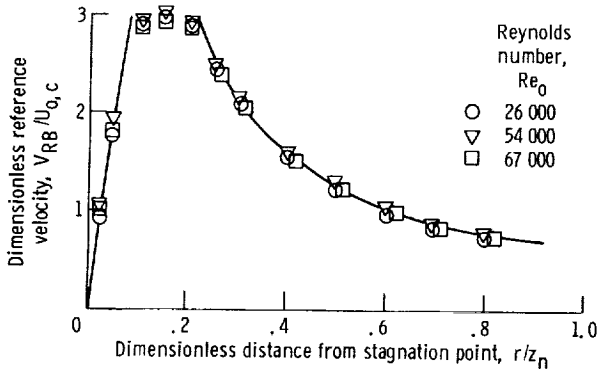

Figure 17. - Reference velocity distribution. Dimensionless nozzle-to-plate spacing, 20; nozzle diameter, 0.250 inch (0.635 cm).

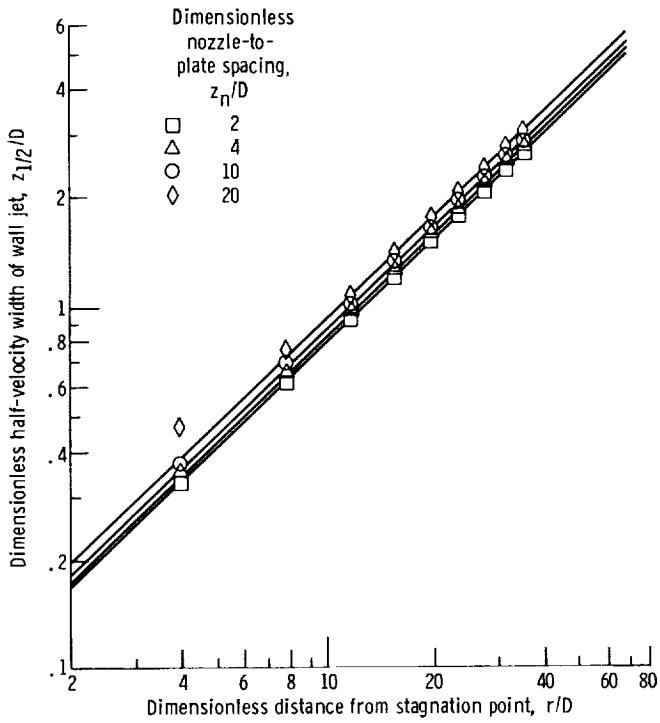

Figure 18. - Spread of wall jet. Nozzle diameter, 0.125 inch (0.317 cm).

where the following constants have been determined experimentally:

$$0.1025 \quad \text{for} \quad \frac{z_n}{D} = 20$$

$$0.0945 \quad \text{for} \quad \frac{z_n}{D} = 10$$

$$0.088 \quad \text{for} \quad \frac{z_n}{D} = 2$$

From these values, K can be represented by

$$K = 0.00081 \frac{z_n}{D} + 0.0864 \tag{19}$$

The spread of the wall jet can then be expressed in general form as

$$\frac{z_{1/2}}{D} = \left(0.00081\,\frac{z_n}{D} + 0.0864\right)\left(\frac{r}{D}\right)^{0.95} \tag{20}$$

Previous investigators obtained the following values for the exponent of r/D: Poreh et al., 0.9; Bakke, 0.94; and Brady and Ludwig, 1.025. Glauert obtained a theoretical value for the exponent of 1.015. The results of the present investigation agree very well with those of Bakke. Bakke's wall jet was generated by means of a radial slot, whereas the wall jet of the present experiment was generated from an impinging circular jet.

In the inner region of the wall jet flow, experimental findings indicate that the exponent in equation (11) changes with Reynolds number and position from 1/7.5 to 1/15 through the range of Reynolds numbers investigated. In other words, the assumption of 1/7 velocity profile for the inner boundary layer, as sometimes done (e.g., in ref. 3), is incorrect. This result indicates, also, that, in the inner boundary layer, similarity can be only approximately realized, in agreement with Glauert's prediction.

Comparison of flow characteristics between unheated smooth plate and steam-heated iron-based alloy. - A series of flow tests was run with the original smooth plate replaced by a segmented plate made with six concentric rings. The segmented plate was steam heated from the bottom so that the plate surface adjacent to the wall jet was approximately 100° F (311 K) above the temperature of the wall jet.

For a nozzle diameter of 0.125 inch (0.317 cm), values of z_n/D of 7 and 14, and a range of Reynolds numbers, the maximum velocity decay along the plate, the velocity profile, and the boundary layer thickness were investigated. No discernible difference existed between the flow properties of the heated plate and the corresponding values for the unheated plate.

SUMMARY OF RESULTS

The experimental flow characteristics of a circular air jet impinging on a flat plate were investigated. The following results were obtained:

1. The length of the potential core is a function of the nozzle exit Reynolds number for laminar flow and is independent of the nozzle exit Reynolds number for a fully developed turbulent circular jet. For nozzle diameters of 0.125, 0.250, and 0.375 inch (0.317, 0.635, and 0.952 cm), the potential core length increased as the nozzle exit Reynolds number increased through the laminar range and reached a maximum at 1000. The potential core length abruptly decreased as the nozzle exit Reynolds number increased beyond 1000, reached a minimum, and then increased only slightly up to a value of about 10 000. For values greater than 10 000, the potential core length is essentially independent of the nozzle exit Reynolds number. The minimum value of the potential core

length decreased with increasing nozzle diameter. For values of the nozzle exit Reynolds number greater than 10 000, the effect of the nozzle diameter on potential core length was insignificant. For fully developed turbulent flow, the experimental value of the potential core length varied from about 6.0 to about 6.7.

2. Static pressures along the impingement plate in the deflection region are dependent on the nozzle-to-plate spacing and less dependent on nozzle diameter and nozzle Reynolds number. The pressures reach a maximum at the stagnation point, decrease rather abruptly with radial distance, and asymptotically approach ambient pressure.

3. A theoretical derivation for the maximum velocity decay for a radial wall jet was developed. This derivation predicts that the decay of the maximum velocity of the wall jet is more rapid than that of a free jet. The theoretical derivation was substantiated by experimental data.

4. An experimental correlation for the spread of the wall jet, where the jet velocity is one-half of the maximum velocity, was presented. The correlation is dependent on the nozzle-to-plate spacing.

5. The nozzle-to-plate spacing has less effect on the boundary layer thickness in the wall jet region than in the vicinity of the stagnation point.

6. No discernible difference existed between the data of a heated plate and that of an unheated plate with respect to boundary layer thickness, velocity profile, and maximum velocity decay rate. The heated plate was allowed to attain a temperature of approximately 100° F (311 K) above the wall jet temperature.

7. The results showed that similarity can only approximately hold in the transition region between the laminar and turbulent flow, since the potential core becomes dependent on the size of the nozzles. Likewise, in the inner boundary layer of the wall jet, a considerable dependence of the velocity profile on position and on the Reynolds number contributes to a weakening of the principle of similarity.

Lewis Research Center,
National Aeronautics and Space Administration,
Cleveland, Ohio, November 10, 1969,
720-03.

APPENDIX A

SYMBOLS

a	constant
a^*	$aD/U_{o,c}$
B	width of potential core
b	half-width of jet
b_o	depth of control volume at r_o
$\overline{b}$	b/D
C_2	dimensionless potential core length for circular jet
D	nozzle diameter
K	constant
k	δ/b
$\overline{L}$	experimental constant
n	exponent
p	static pressure
p'	total pressure
Re_o	Reynolds number based on nozzle exit velocity and either nozzle diameter or slot width
r	distance from stagnation point in radial direction
r_o	distance from stagnation point to front face of control volume
$\overline{r}$	r/D
$\overline{r}_o$	r_o/D
U	velocity in axial direction
V	velocity in radial direction
V_o	velocity in radial direction at r_o
V_{RB}	reference velocity
$\overline{V}$	$V/U_{o,c}$
$\overline{V}_m$	$V_m/U_{o,c}$
x	distance from nozzle in axial direction
x_c	absolute potential core length
y	distance from centerline in radial direction
$y_{1/2}$	value of y for which $U = \frac{1}{2} U_m$
z	distance from impingement plate in axial direction
z_n	distance between nozzle and impingement plate
$\overline{z}$	z/δ
$z_{1/2}$	value of z for which $V = \frac{1}{2} V_m$
α	constant
α_1	$(\alpha + 1)\beta/2$
$\beta/2$	$\dfrac{\frac{kn}{n+1} + 0.31559}{\frac{kn}{n+1} + 2(0.31559)}$
δ	boundary layer thickness
$\overline{\delta}$	δ/D
ϵ	virtual kinematic viscosity
ζ	$\dfrac{z - \delta}{b}$
$\zeta_{1/2}$	$\dfrac{z_{1/2} - \delta}{b}$
ρ	density
τ	turbulent shearing stress

Subscripts:

m	centerline or maximum	o, c	centerline nozzle exit
o	average nozzle exit	λ	ambient

APPENDIX B

MAXIMUM VELOCITY DECAY OF RADIAL WALL JET

By a method similar to that used by Abramovich for two-dimensional wall jets, an expression is derived herein for the maximum velocity decay of a radial wall jet. The coordinate system used in the following and the control volume 1234 considered for making the momentum balance are shown in figure 19. The conservation of momentum for this control volume may be written as

(momentum into 12) + (momentum into 23) - (momentum out 14)

- (momentum out 43) = (momentum accumulated in 1234)

This equation is valid only if the turbulent shearing stress $\tau = 0$ for $V = V_m$. For turbulent flow, this assumption is in agreement with Prandtl's theory. Recently, measurements made by Poreh et al., for example, indicate that $\tau \neq 0$ for $V = V_m$.

Under the assumptions that ρ is constant, that the flow is steady state, and that the ambient fluid is at rest, the second term on the left and the term on the right in the conservation of momentum equation vanish. The equation may then be written as

$$2\pi r_o b_o \rho V_o^2 - \int_{r_o}^{r} \rho V_m \frac{d}{dr}\left(\int_0^{\delta} 2\pi r V \, dz\right) dr = \int_{\delta}^{\delta+b} 2\pi r \rho V^2 \, dz \tag{B1}$$

Removing the constant $2\pi\rho$ and differentiating equation (B1) with respect to r give

$$V_m \frac{d}{dr}\int_0^{\delta} Vr \, dz + \frac{d}{dr}\int_{\delta}^{\delta+b} V^2 r \, dz = 0 \tag{B2}$$

To make the parameters dimensionless, set

$$\bar{V} = \frac{V}{U_{o,c}}, \quad \bar{V}_m = \frac{V_m}{U_{o,c}}, \quad \bar{z} = \frac{z}{\delta}, \quad \zeta = \frac{z-\delta}{b}, \quad \bar{r} = \frac{r}{D}, \quad \bar{b} = \frac{b}{D}, \quad \bar{\delta} = \frac{\delta}{D} \tag{B3}$$

and obtain from equation (B2)

$$\bar{V}_m \frac{d}{dr}\int_0^{1} \bar{V}\bar{r}D^2\bar{\delta} \, d\bar{z} + \frac{d}{dr}\int_0^{1} \bar{V}^2\bar{r}D^2\bar{b} \, d\zeta = 0 \tag{B4}$$

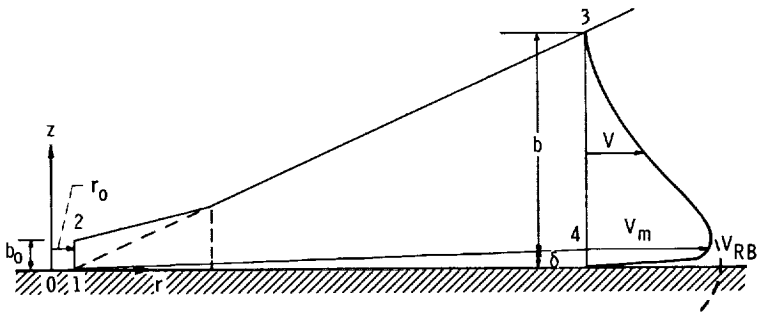

Figure 19. - Coordinate system of radial wall jet.

In the boundary layer, the velocity distribution may be expressed by the well-known power law for turbulent flow:

$$\overline{V} = \overline{V}_m(\overline{z})^{1/n} \qquad 0 < \overline{z} < 1 \tag{B5}$$

Outside the boundary layer, it has been shown in this report that the velocity distribution may be expressed by

$$\overline{V} = \overline{V}_m\left(1 - \zeta^{3/2}\right)^2 \qquad 0 < \zeta < 1 \tag{B6}$$

Insert equations (B5) and (B6) into equation (B4), and replace d/dr by $(1/D)(d/d\overline{r})$ to find

$$\overline{V}_m \frac{d}{d\overline{r}} \int_0^1 \overline{V}_m \overline{r}\overline{\delta}\overline{z}^{1/n}\, d\overline{z} + \frac{d}{d\overline{r}} \int_0^1 \overline{V}_m^2 \overline{r}\overline{b}\left(1 - \zeta^{3/2}\right)^4 d\zeta = 0 \tag{B7}$$

Now,

$$\int_0^1 \overline{z}^{1/n}\, d\overline{z} = \frac{n}{n+1}$$

$$\int_0^1 \left(1 - \zeta^{3/2}\right)^4 d\zeta = 0.31559 \tag{B8}$$

With the use of equation (B8), equation (B7) becomes

$$\frac{n}{n+1} \overline{V}_m \frac{d}{d\overline{r}} \left(\overline{V}_m \overline{r}\overline{\delta}\right) + 0.31559 \frac{d}{d\overline{r}} \left(\overline{V}_m^2 \overline{r}\overline{b}\right) = 0 \tag{B9}$$

Perform the indicated operations to find

$$\frac{n}{n+1}\bar{V}_m^2\bar{r}\bar{\delta}' + \frac{n}{n+1}\bar{V}_m^2\bar{\delta} + \frac{n}{n+1}\bar{V}_m\bar{V}_m'\bar{r}\bar{\delta} + 0.31559\,\bar{V}_m^2\bar{r}\bar{b}' + 0.31559\,\bar{V}_m^2\bar{b}$$

$$+ 0.31559(2)\bar{V}_m\bar{V}_m'\bar{r}\bar{b} = 0 \qquad \text{(B10)}$$

Equation (B10) becomes, on division by $\bar{b}\bar{r}\bar{V}_m^2$,

$$\frac{n}{n+1}\frac{\bar{\delta}'}{\bar{b}} + \frac{n}{n+1}\frac{1}{\bar{r}}\frac{\bar{\delta}}{\bar{b}} + \frac{\bar{V}_m'}{\bar{V}_m}\frac{\bar{\delta}}{\bar{b}}\frac{n}{n+1} + 0.31559\,\frac{\bar{b}'}{\bar{b}} + 0.31559\,\frac{1}{\bar{r}} + 2(0.31559)\frac{\bar{V}_m'}{\bar{V}_m} = 0 \qquad \text{(B11)}$$

Let $\bar{\delta} = k\bar{b}$ where $0 < k < 1$ and $\bar{b} = \bar{L}(\bar{r} - \bar{r}_o)^{\alpha}$, as suggested by the experimental results; then, equation (B11) may be written as

$$\left(\frac{kn}{n+1} + 0.31559\right)\frac{\bar{b}'}{\bar{b}} + \left(\frac{kn}{n+1} + 0.31559\right)\frac{\bar{r}'}{\bar{r}} + \left[\frac{kn}{n+1} + 2(0.31559)\right]\frac{\bar{V}_m'}{\bar{V}_m} = 0 \qquad \text{(B12)}$$

Set

$$\frac{\dfrac{kn}{n+1} + 0.31559}{\dfrac{kn}{n+1} + 2(0.31559)} = \frac{\beta}{2}$$

and integrate to find

$$\frac{\beta}{2}\ln\bar{b} + \frac{\beta}{2}\ln\bar{r} + \ln\bar{V}_m = \ln \text{constant}$$

or

$$\bar{V}_m = \frac{\text{constant}}{(\bar{b}\bar{r})^{\beta/2}} \qquad \text{(B13)}$$

$$\bar{V}_m = \frac{\text{constant}}{\left[\bar{L}\bar{r}^{\alpha}\left(1 - \dfrac{\bar{r}_o}{\bar{r}}\right)^{\alpha}\bar{r}\right]^{\beta/2}}$$

$$= \frac{\text{constant}}{\bar{r}^{(\alpha+1)\beta/2}\left(1 - \dfrac{\bar{r}_o}{\bar{r}}\right)^{\alpha\beta/2}} \qquad \text{(B14)}$$

For $\overline{r}_o \ll r$,

$$\overline{V}_m = \frac{\text{constant}}{\overline{r}^{\alpha_1}} \tag{B15}$$

where

$$\alpha_1 = \frac{(\alpha + 1)\beta}{2}$$

REFERENCES

1. Gauntner, J. W.; Livingood, J. N. B.; and Hrycak, Peter: Survey of Literature on Flow Characteristics of a Single Turbulent Jet Impinging on a Flat Plate. NASA TN D-5652, 1969.

2. Lee, David T.-H.: Experimental Investigation of Submerged Incompressible Turbulent Impinging Jets. M.S. Thesis, Newark College of Eng., 1969.

3. Abramovich, Genrikh N.: The Theory of Turbulent Jets. MIT Press, 1963.

4. Albertson, M. L.; Dai, Y. B.; Jensen, R. A.; and Rouse, Hunter: Diffusion of Submerged Jets. ASCE Trans., vol. 115, 1950, pp. 639-697.

5. Tani, I.; and Komatsu, Y.: Impingement of a Round Jet on a Flat Surface. Applied Mechanics. Henry Görtler, ed., Springer-Verlag, 1966, pp. 672-676.

6. Tollmien, Walter: Calculation of Turbulent Expansion Processes. NACA TM 1085, 1945.

7. Görtler, H.: Berechnung von Augfaben der freien Turbulenz auf Grund eines neuen Naherungsansatzes. Z. angew. Math. Mech., vol. 22, no. 5, Oct. 1942, pp. 244-254.

8. Miller, David R.; and Comings, Edward W.: Static Pressure Distribution in the Free Turbulent Jet. J. Fluid Mech., vol. 3, pt. 1, Oct. 1957, pp. 1-16.

9. Schlichting, Hermann (J. Kestin, trans.): Boundary Layer Theory. Sixth ed., McGraw-Hill Book Co., Inc., 1968.

10. Poreh, Michael; and Cermak, J. E.: Flow Characteristics of a Circular Submerged Jet Impinging Normally on a Smooth Boundary. Presented at the Sixth Midwestern Conference on Fluid Mechanics, Univ. of Texas, 1959.

11. Brady, W. Gordon; and Ludwig, G.: Theoretical and Experimental Studies of Impinging Uniform Jets. J. Am. Helicopter Soc., vol. 8, no. 2, 1963, pp. 1-13.

12. Bakke, P.: An Experimental Investigation of a Wall Jet. J. Fluid Mech., vol. 2, pt. 5, July 1957, pp. 467-472.

13. Glauert, M. B.: The Wall Jet. J. Fluid Mech., vol. 1, pt. 6, Dec. 1956, pp. 625-643.

NASA-Langley, 1970 —— 12 E-5239